Ji et al. Biomarker Research (2026) 14:7
https://doi.org/10.1186/s40364-025-00876-x

Biomarker Research

CORRESPONDENCE Open Access

Spatial multi-omics mapping of tumor microanatomy dynamics following radiotherapy combined with targeted-immunotherapy in hepatocellular carcinoma

Fansen Ji[1,2,3,4†], Haoming Xia[2,3,4†], Ying Xiao[5†], Jiawei Zhang[6†], Hao Chen[2,3,4], Bingjun Tang[2,3,4], Huan Li[5], Hao Liu[5], Boyang Wu[2,3,4], Xiaojuan Wang[2,3,4], Shizhong Yang[2,3,4*] and Jiahong Dong[2,3,4*]

Abstract

Remodeling of the tumor microenvironment (TME) under therapeutic pressure is a critical determinant of treatment response and resistance in hepatocellular carcinoma (HCC). Triple-combination therapy integrating targeted agents, immune checkpoint inhibitors, and radiotherapy (T+I+R) has shown potential synergistic effects in intermediate to advanced HCC, particularly in patients with portal vein tumor thrombus (PVTT), yet the spatial and cellular mechanisms underlying its efficacy remain largely unknown. In this retrospective clinical cohort study, we compared T+I+R with targeted therapy plus radiotherapy (T+R) in advanced HCC, and further employed single-cell spatial transcriptomics and spatial proteomics to generate an integrated multi-omics atlas mapping tumor and stromal compartments, cellular compositions, and intercellular interactions with spatial resolution. Clinically, T+I+R achieved superior tumor shrinkage and disease control compared with T+R. Spatial multi-omics revealed marked region-specific remodeling, with myofibroblastic cancer-associated fibroblasts, angiogenic tip endothelial cells, and conventional dendritic cells enriched at the invasive margin and associated with therapeutic resistance, while $CD8^+$ effector T cells were redistributed away from immunosuppressive niches, a spatial configuration correlating with enhanced response. These findings identify spatial segregation between cytotoxic and suppressive immune elements as a potential hallmark of effective therapy, providing a high-resolution spatial framework for understanding T+I+R induced TME remodeling and offering mechanistic insights to guide biomarker discovery and the optimization of combination strategies in advanced HCC.

†Fansen Ji, Haoming Xia, Ying Xiao and Jiawei Zhang contributed equally.

*Correspondence:
Shizhong Yang
ysza02008@btch.edu.cn
Jiahong Dong
dongjiahong@tsinghua.edu.cn
[1]Tsinghua-Peking Center for Life Sciences, Tsinghua University, Beijing 102218, China
[2]School of Clinical Medicine, Tsinghua University, Beijing 102218, China
[3]Hepatopancreatobiliary Center, Beijing Tsinghua Changgung Hospital, Key Laboratory of Digital Intelligence Hepatology (Ministry of Education), School of Clinical Medicine, Tsinghua Medicine, Tsinghua University, Beijing 102218, China
[4]Research Unit of Precision Hepatobiliary Surgery Paradigm, Chinese Academy of Medical Sciences, Beijing, China
[5]Department of Pathology, Beijing Tsinghua Changgung Hospital, Tsinghua University, Beijing 102218, China
[6]Health Management Center, Beijing Jishuitan Hospital, Capital Medical University, Beijing 100035, China

To the editor,

Radiotherapy (RT) has expanded local treatment options for non-surgical HCC and can remodel the TME to potentiate systemic therapies. [1–5] Dissecting the multicellular organization within tissue niches provides critical insights into the pathological behavior of cancer and its response to therapy. [6–8] We retrospectively evaluated a triple-combination regimen of external beam RT (EBRT), Lenvatinib and anti-PD-1 antibody (T+I+R) versus EBRT plus Lenvatinib (T+R) in 208 patients (156 T+I+R, 52 T+R, Fig. 1A, Fig. S1). The T+I+R group showed higher objective response and disease control rates for both tumor and PVTT (Fig. 1B, Table S2, Fig. S2A, B), and significantly improved median overall and progression-free survival in the full cohort and after 1:2 propensity score matching (Fig. 1C–F, Fig. S2C, D), supporting a clinical benefit of adding immune checkpoint blockade to targeted therapy and radiotherapy.

To dissect the tissue-level basis of this benefit, we generated a spatial multi-omics atlas using surgical specimens from 4 treated neoadjuvantly with T+I+R and 7 treatment-naïve HCC patients (Fig. 1G, Table S2). Spatial transcriptomics (CosMx SMI; ~1,000 genes, 31 tissue microarray (TMA) cores totally, Table S3) and spatial proteomics (GeoMx Immuno-Oncology assay; > 570 proteins across 39 regions of interest (ROIs), Table S4) together produced high-resolution maps comprising 171,332 segmented single cells across tumor core (T), invasive margin (B), and peritumoral area (N). Meanwhile, patients under T+I+R treatment were divided into responders (R) and Nonresponder (NR) based on the mRECIST criteria. Cells were clustered into eight major lineages (tumor, hepatocytes, Hepatic stellate cells (HSCs), endothelial, myeloid, cholangiocytes, T/NK, B/plasma), enabling systematic interrogation of spatial and compositional changes after therapy (Fig. 1H, Fig. S3A-D, Table S5). We found T+I+R was associated with increased frequencies of myeloid cells, T/NK cells and B/plasma populations, consistent with therapy-induced immune activation; however, immune cell enrichment was heterogeneously distributed and in our small treated series, appeared greater in non-responders (Fig. 1I). Further subtyping of each lineage helps us to define the precise location of each cell with HCC under the treatment of T+I+R coupled with matched Immunofluorescence images (Fig. 1J, Fig. S5-7). Spatial transcriptomics analysis further revealed a trend toward immune cell and HSCs accumulation at invasive margins, though this did not reach statistical significance (Fig. S3E). Morphological segmentation of spatial proteomics data (α-SMA+/CK8/18+/CD45+) showed a stromal enrichment within tumor ROIs (Fig. 1K, L). Differential protein analysis further revealed that tumoral regions in responders showed increased activity in lymphocyte recruitment and immune activation pathways (Fig. 1M, Fig. S4), reflecting an enhanced immune cell engagement.

Next, three aspects of comparisons were performed within different subtypes of CAFs, endothelial cells and myeloid cells: 1) Naive and T+I+R cohort; 2) T, B and N regions; 3) responders and nonresponders. We revealed a stereotyped remodeling at the invasive margin: myofibroblastic cancer-associated fibroblasts (mCAFs), angiogenic tip endothelial cells and conventional dendritic cells were concentrated at the front and associated with therapeutic resistance (Fig. 2A–I, Fig. S5-7, Table S6-8). Tumor composition was remodeled following treatment, with expansion of two resistant tumor subtypes (marked by ANXA2 and CXCL10 expression) that localized to the invasive front and were enriched in non-responders (Fig. 2J–O, Table S9), while different clusters with implications with patients' prognosis (Fig. S8). [9, 10] Neighborhood analyses showed reduced densities of mCAFs, tumor cells and Mono/Mph populations adjacent to $CD8^+$ Teff cells after T+I+R, coupled with increased association of $CD8^+$ cells with antigen-presenting/stimulatory compartments (aCAFs, plasma cells) and exhausted phenotypes, indicating a shift in $CD8^+$ microenvironments toward less fibrotic, more immune-permissive states in responders (Fig. 2P, Q). Unsupervised spatial niche analysis within TME identified seven recurrent multicellular niches (Fig. 2R, S) with distinct cell type enrichment, and post-treatment patients were preferentially occupied by immune-associated niches (iCAFs_Immune, B/Plasma, CD8_CD4_DCs, Vascular), underscoring therapy-induced restructuring of the immune landscape (Fig. 2T).

Collectively, these clinical and spatial multi-omics data indicate the clinical value of T+I+R for HCC treatment, which may induce extensive, region-specific remodeling of the HCC TME. Spatial organization of immune and stromal elements, particularly the emergence of immune-enriched niches and the reduction of pericellular fibrosis, may serve as a hallmark of therapeutic responsiveness. Limitations include the retrospective design, small spatial cohort, and potential sampling bias of TMA cores, as well as the patient-specific bias introduced by having only one responder case. Additional whole-section validation would further enhance the robustness of our findings. Prospective validation is warranted to translate these spatial signatures into predictive biomarkers and to refine combination strategies. [11, 12]

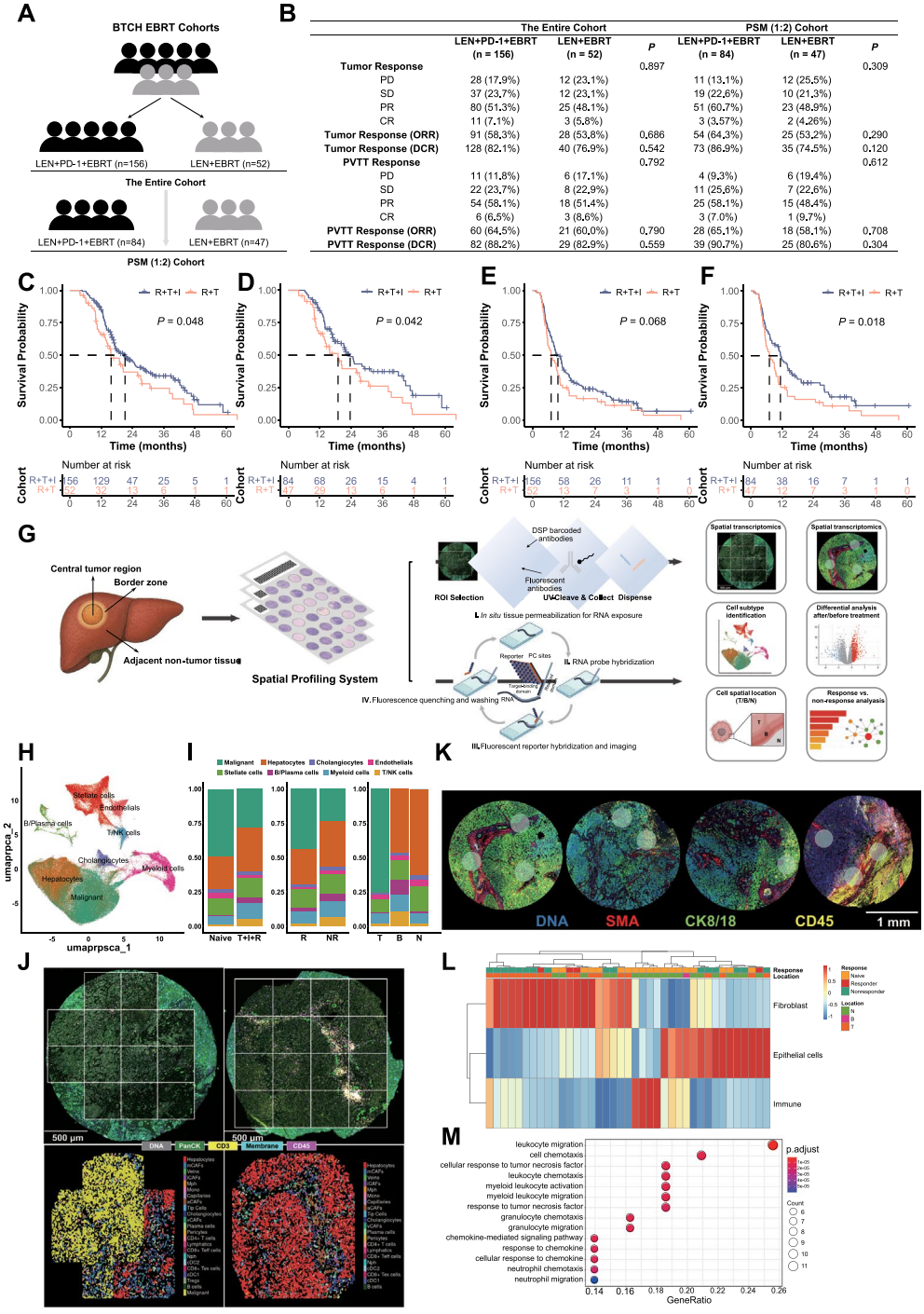

	The Entire Cohort			PSM (1:2) Cohort		
	LEN+PD-1+EBRT (n = 156)	LEN+EBRT (n = 52)	*P*	LEN+PD-1+EBRT (n = 84)	LEN+EBRT (n = 47)	*P*
Tumor Response			0.897			0.309
PD	28 (17.9%)	12 (23.1%)		11 (13.1%)	12 (25.5%)	
SD	37 (23.7%)	12 (23.1%)		19 (22.6%)	10 (21.3%)	
PR	80 (51.3%)	25 (48.1%)		51 (60.7%)	23 (48.9%)	
CR	11 (7.1%)	3 (5.8%)		3 (3.57%)	2 (4.26%)	
Tumor Response (ORR)	91 (58.3%)	28 (53.8%)	0.686	54 (64.3%)	25 (53.2%)	0.290
Tumor Response (DCR)	128 (82.1%)	40 (76.9%)	0.542	73 (86.9%)	35 (74.5%)	0.120
PVTT Response			0.792			0.612
PD	11 (11.8%)	6 (17.1%)		4 (9.3%)	6 (19.4%)	
SD	22 (23.7%)	8 (22.9%)		11 (25.6%)	7 (22.6%)	
PR	54 (58.1%)	18 (51.4%)		25 (58.1%)	15 (48.4%)	
CR	6 (6.5%)	3 (8.6%)		3 (7.0%)	1 (9.7%)	
PVTT Response (ORR)	60 (64.5%)	21 (60.0%)	0.790	28 (65.1%)	18 (58.1%)	0.708
PVTT Response (DCR)	82 (88.2%)	29 (82.9%)	0.559	39 (90.7%)	25 (80.6%)	0.304

Fig. 1 Treatment outcomes and spatial transcriptomic features of HCC under neoadjuvant LEN+PD-1+EBRT. (**A**) Schematic diagram illustrating patient grouping for the entire and 1:2 PSM cohorts. (**B**) Treatment response rates including ORR and DCR for tumor and PVTT in the entire and 1:2 PSM cohorts. (**C-F**) Kaplan-Meier curves depicting OS (**C**) and PFS (**D**) in the entire cohort, OS (**E**) and PFS (**F**) in the 1:2 PSM cohort between LEN+PD-1+EBRT and EBRT groups. (**G**) Schematic overview of experimental workflow. (**H**) UMAP visualization of single cell clustering analysis based on spatial transcriptomics data. Colors correspond to distinct transcriptional clusters. (**I**) Left, Cellular fraction comparisons between treatment-naïve (Naïve) and T+I+R groups. Middle, Cellular fraction comparisons between responders (R) vs. non-responders (NR) under T+I+R. Right, Cellular fraction comparisons between tumor core (T), invasive margin (B), and peritumoral area (N). (**J**) Representative spatial mapping images visualizing the localization and spatial distribution of major cell types in tissue sections. (**K**) Representative IF staining images of multiplex DSP overlays from tumor ROIs. (**L**) Heatmap of cell-type abundances (CAF, epithelial, immune) derived from morphological segmentation (α-SMA$^+$/CK8/18$^+$/CD45$^+$), annotated by ROI location (N/B/T) and response status (R/NR). (**M**) Dot plot of immune-related pathways significantly upregulated in peritumoral regions of responders; x-axis shows $-\log_2$(adjusted *P*)

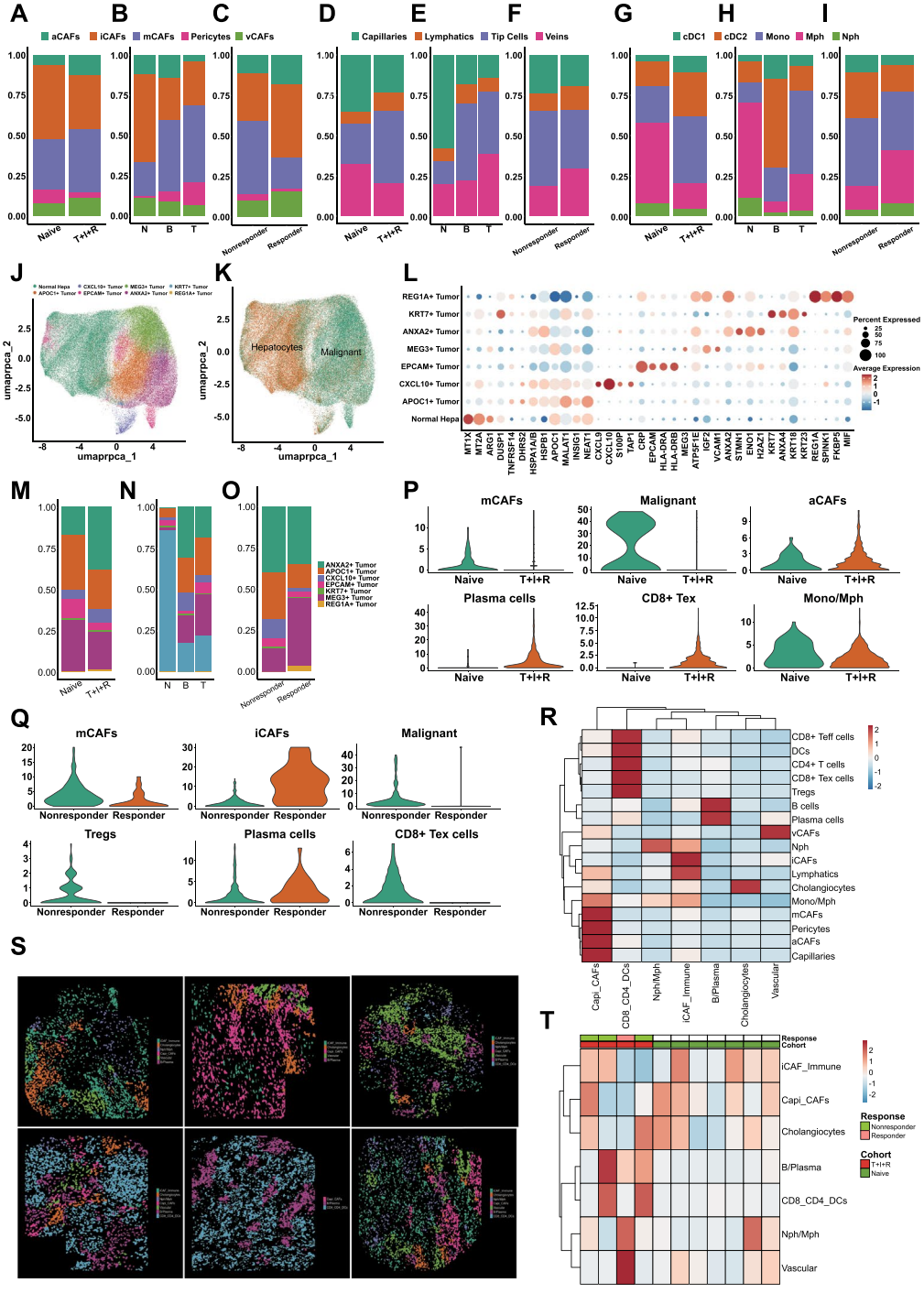

Fig. 2 (See legend on next page.)

(See figure on previous page.)

Fig. 2 Spatial niche remodeling and CD8$^+$ T cell-centered microenvironment dynamics in HCC following LEN+PD-1+EBRT therapy. (**A**) Stacked bar chart comparing the relative proportions of each CAF subtype in treatment-naïve (Naive) versus T+I+R–treated tumors. (**B**) Stacked bar chart comparing the relative proportions of each CAF subtype across spatial regions: tumor core (T), invasive margin (B), and peritumoral area (N). (**C**) Stacked bar chart of CAF subtype proportions in non-responders (NR) versus responders (R). (**D-F**) The same analysis performed on endothelial subtypes. (**G-I**) The same analysis performed on myeloid cell subtypes. (**J**, **K**) UMAP plot of all epithelial cells from single-cell transcriptomes highlighting seven malignant subpopulations and one normal hepatocyte cluster. (**L**) Dot plot depicting the expression of canonical marker genes. (**M**) Stacked bar plots showing proportional changes in malignant subpopulations pre- and post-T+I+R therapy. (**N**) Stacked bar plot of malignant subpopulations across tumor core (T), invasive margin (B), and peritumoral area (N), demonstrating preferential localization of resistant subtypes at the invasive front. (**O**) Stacked Bar plot comparing the abundance of malignant subpopulations in responders versus non-responders, showing enrichment of therapy-resistant subtypes in non-responders. (**P**) Violin plots illustrating the local spatial composition of CD8$^+$ Teff neighborhoods in naïve and T+I+R-treated groups. (**Q**) Violin plots comparing the spatial density of major cell types in CD8$^+$ Teff neighborhoods between responders and nonresponders post-treatment. (**R**) Heatmap of seven major spatial multicellular niches identified by unsupervised neighborhood analysis excluding malignant and hepatocyte populations. (**S**) Representative spatial maps visualizing the localization of identified multicellular niches within HCC tissue sections. (**T**) Heatmap comparing the enrichment of spatial niches between responders and non-responders, as well as between naïve and post-T+I+R-treated cohorts

Supplementary information

The online version contains supplementary material available at https://doi.org/10.1186/s40364-025-00876-x.

Supplementary Material 1

Supplementary Material 2

Supplementary Material 3

Acknowledgements
The authors would like to acknowledge the assistance of Imaging Core Facility, Technology Center for Protein Sciences, Tsinghua University for assistance of using CosMx SMI instrument/software.

Author contributions
Conception and design: J.H.D and S.Z.Y.; Development of methodology: F.S.J., H.M.X., and X.J.W.; Acquisition of data: F.S.J. and H.M.X.; Data analysis and interpretation: F.S.J., H.M.X. and J.W.Z.; Figure preparation: F.S.J., H.M.X. H.C., Y.X., B.J.T., H.L., H.L., and B.Y.W.; Writing the manuscript: F.S.J. and H.M.X.; Study supervision: J.H.D, S.Z.Y. and X.J.W.; All authors read and approved the final version of the manuscript.

Funding
This work was supported by the Natural Science Foundation of China (82090052, 82090050, and 82090053), CAMS Innovation Fund for Medical Sciences (2019-I2M-5-056) and Tsinghua University Initiative Scientific Research Program of Precision Medicine (2022ZLA007).

Data availability
The datasets used and analyzed in this study are available from the corresponding author on reasonable request.

Declarations

Ethical approval
This study was approved by the Institutional Review Board (IRB) of Beijing Tsinghua Changgung Hospital, Tsinghua University (Approval No. 21323–0-01). All participants provided written informed consent in accordance with the Declaration of Helsinki.

Consent for publication
Not applicable.

Competing interests
The authors declare no competing interests.

Received: 11 August 2025 / Accepted: 13 November 2025
Published online: 08 January 2026

References

1. Galluzzi L, Aryankalayil MJ, Coleman CN, Formenti SC. Emerging evidence for adapting radiotherapy to immunotherapy. Nat Rev Clin Oncol. 2023;20:543–57. https://doi.org/10.1038/s41571-023-00782-x.
2. Li Z, Liu J, Zhang B, Yue J, Shi X, Cui K, Liu Z, Chang Z, Sun Z, Li M, et al. Neoadjuvant tislelizumab plus stereotactic body radiotherapy and adjuvant tislelizumab in early-stage resectable hepatocellular carcinoma: the notable-HCC phase 1b trial. Nat Commun. 2024;15:3260. https://doi.org/10.1038/s41467-024-47420-3.
3. Topalian SL, Forde PM, Emens LA, Yarchoan M, Smith KN, Pardoll DM. Neoadjuvant immune checkpoint blockade: a window of opportunity to advance cancer immunotherapy. Cancer Cell. 2023;41:1551–66. https://doi.org/10.1016/j.ccell.2023.07.011.
4. Dudzinski SO, Newman NB, McIntyre J, Engineer R, Sanford NN, Wo JY, Seong J, Guha C, Chang DT, Hong TS, et al. Emerging evidence-based role for external-beam radiation therapy in hepatocellular carcinoma. Lancet Gastroenterol Hepatol. 2025;10:387–98. https://doi.org/10.1016/S2468-1253(24)00267-X.
5. Wei X, Jiang Y, Zhang X, Feng S, Zhou B, Ye X, Xing H, Xu Y, Shi J, Guo W, et al. Neoadjuvant three-dimensional conformal radiotherapy for resectable hepatocellular carcinoma with portal vein tumor thrombus: a randomized, open-label, multicenter controlled study. J Clin Oncol. 2019;37:2141–51. https://doi.org/10.1200/JCO.18.02184.
6. Shi Q, Chen Y, Li Y, Qin S, Yang Y, Gao Y, Zhu L, Wang D, Zhang Z. Cross-tissue multicellular coordination and its rewiring in cancer. Nature. 2025;1–10. https://doi.org/10.1038/s41586-025-09053-4.
7. Pelka K, Hofree M, Chen JH, Sarkizova S, Pirl JD, Jorgji V, Bejnood A, Dionne D, Ge WH, Xu KH, et al. Spatially organized multicellular immune hubs in human colorectal cancer. Cell. 2021;184:4734–52.e20. https://doi.org/10.1016/j.cell.2021.08.003.
8. Hwang WL, Jagadeesh KA, Guo JA, Hoffman HI, Yadollahpour P, Reeves JW, Mohan R, Drokhlyansky E, Van Wittenberghe N, Ashenberg O, et al. Single-nucleus and spatial transcriptome profiling of pancreatic cancer identifies multicellular dynamics associated with neoadjuvant treatment. Nat Genet. 2022;54:1178–91. https://doi.org/10.1038/s41588-022-01134-8.
9. Limagne E, Nuttin L, Thibaudin M, Jacquin E, Aucagne R, Bon M, Revy S, Barnestein R, Ballot E, Truntzer C, et al. MEK inhibition overcomes chemoimmunotherapy resistance by inducing CXCL10 in cancer cells. Cancer Cell. 2022;40:136–52.e12. https://doi.org/10.1016/j.ccell.2021.12.009.
10. Matchett KP, Wilson-Kanamori JR, Portman JR, Kapourani CA, Fercoq F, May S, Zajdel E, Beltran M, Sutherland EF, Mackey JBG, et al. Multimodal decoding of human liver regeneration. Nature. 2024;630:158–65. https://doi.org/10.1038/s41586-024-07376-2.
11. Lewis SM, Asselin-Labat M-L, Nguyen Q, Berthelet J, Tan X, Wimmer VC, Merino D, Rogers KL, Naik SH. Spatial omics and multiplexed imaging to explore cancer biology. Nat Methods. 2021;18:997–1012. https://doi.org/10.1038/s41592-021-01203-6.

12. Walker C, Angelo M. Toward clinical applications of spatial-omics in cancer research. Nat Cancer. 2024;5:1771–73. https://doi.org/10.1038/s43018-024-00868-0.

Publisher's Note